Ultrafast Vibrational Dynamics of Water Disentangled by Reverse Nonequilibrium *Ab Initio* Molecular Dynamics Simulations

Yuki Nagata,[*] Seiji Yoshimune, Cho-Shuen Hsieh, Johannes Hunger, and Mischa Bonn

Max-Planck Institute for Polymer Research, Ackermannweg 10, D-55128, Mainz, Germany
(Received 22 July 2014; revised manuscript received 31 January 2015; published 1 April 2015)

Water is a unique solvent with strong, yet highly dynamic, intermolecular interactions. Many insights into this distinctive liquid have been obtained using ultrafast vibrational spectroscopy of water's O-H stretch vibration. However, it has been challenging to separate the different contributions to the dynamics of the O-H stretch vibration in H_2O. Here, we present a novel nonequilibrium molecular dynamics (NEMD) algorithm that allows for a detailed picture of water vibrational dynamics by generating nonequilibrium vibrationally excited states at targeted vibrational frequencies. Our *ab initio* NEMD simulations reproduce the experimentally observed time scales of vibrational dynamics in H_2O. The approach presented in this work uniquely disentangles the effects on the vibrational dynamics of four contributions: the delocalization of the O-H stretch mode, structural dynamics of the hydrogen bonded network, intramolecular coupling within water molecules, and intermolecular coupling between water molecules (near-resonant energy transfer between O-H groups). Our results illustrate that intermolecular energy transfer and the delocalization of the O-H stretch mode are particularly important for the spectral diffusion in H_2O.

I. INTRODUCTION

Water provides a unique environment as a solvent for important chemical reactions, and fluctuations of solute-water interactions govern reaction rates and protein aggregation [1–4]. Ultrafast fluctuation of these solute-water interactions enables dissipation of excess energy released in reaction processes very efficiently, removing the excess energy from reactive sites quickly, thereby preventing possible backreactions. The delocalization and rapid dissipation of high-energy vibrational quanta—specifically the O-H stretch vibration—have been attributed to strong coupling between O-H groups, both between O-H groups within the same molecule (intramolecular coupling) and between O-H groups of different molecules (intermolecular coupling). This strong coupling has been ascribed to the large transition dipole moment of the O-H stretch vibration and has been shown to lead not only to resonant vibrational energy transfer between O-H groups [5] but also to the delocalization of the vibrational amplitude over several O-H groups [6,7]. Understanding the dynamics of energy flow in pure liquid water is essential for obtaining molecular-level insights into the role of water for chemical reactions in aqueous environments and biologically relevant processes.

Experimentally, there have been several attempts to quantify the strength of intramolecular and intermolecular couplings, the rate of vibrational energy transfer between O-H groups, and the degree of delocalization of the vibrational amplitude. One of the most successful approaches uses femtosecond time-resolved vibrational spectroscopy [8–13]. In these time-resolved experiments, a vibrational mode is excited using laser pulses with a specific frequency, and the effect of the excitation is probed over a wide spectral window as a function of time after excitation. The excitation will result in a reduction of the infrared absorption ("bleach") at the excitation frequency, and the excitation energy is transferred to other modes on ultrashort time scales. Through changes in the local environment of the water molecules and/or energy transfer between water molecules, the bleach will change its spectral shape—a phenomenon called spectral diffusion. The spectral diffusion in bulk H_2O is extremely fast (<180 fs [14–16]), and several mechanisms have been suggested to contribute to this fast spectral diffusion. On time scales faster than about 50 fs, the coupling to lower-frequency vibrational modes (e.g., stretching and librational modes) [14–17] results in spectral diffusion. However, this coupling does not very strongly modulate the O-H stretch frequency and thus can only account for spectral diffusion within a relatively narrow frequency range [about 80 cm^{-1} (50 cm^{-1}) for the O-H (O-D) stretching vibration in D_2O (H_2O)] [18]. To fully scramble the initial frequency of an O-H (O-D) stretch oscillator [150 cm^{-1} (110 cm^{-1})] [18], other mechanisms must be at play. In neat H_2O, this loss of frequency memory has been

---

[*]Corresponding author.
nagata@mpip-mainz.mpg.de

reported to occur on time scales of less than 180 fs [14–16]. Interestingly, this spectral diffusion is substantially slower (about 1 ps) in isotopically diluted water (i.e., HDO in D_2O) [19–23]. In the latter system, the O-H stretch vibrations are isolated (i.e., decoupled from other O-H groups), resulting in the elimination of intramolecular or intermolecular energy-transfer paths within O-H stretching modes. Clearly, spectral diffusion is accelerated through the interactions between the O-H stretch chromophores, and as such, it has been used to quantify ultrafast coupling processes in liquid water [5,24,25]. These intramolecular or intermolecular couplings of the O-H chromophores are, amongst others, the result of the dipole-dipole coupling between different O-H stretch transition dipole moments, resulting in Förster-type resonant energy transfer between molecules [26]. Note that intermolecular energy transfer cannot solely account for the fast spectral diffusion in neat H_2O, as the decay of the excitation anisotropy, which is dominated by intermolecular energy transfer, is somewhat slower than the spectral diffusion time [14,15]. Although these intramolecular and intermolecular couplings in H_2O clearly contribute to the acceleration of the spectral diffusion, neither the individual contributions nor the detailed mechanisms have been addressed.

Here, we present a novel molecular dynamics (MD) approach that allows us to quantify spectral diffusion and vibrational energy relaxation *in silico* with *ab initio* molecular dynamics (AIMD) simulations [27,28]. More importantly, our approach allows us to disentangle the different contributions to the overall spectral diffusion process, i.e., vibrational energy delocalization, intramolecular coupling, and intermolecular coupling. In AIMD, the anharmonicities of vibrational modes and the couplings between them, which critically affect the vibrational dynamics, are explicitly taken into account via electronic structure theory, providing an ideal tool to simulate the vibrational dynamics of the O-H stretch mode in bulk H_2O [29,30]. Nevertheless, the lack of a simple algorithm to generate a frequency-resolved nonequilibrium state, including the delocalized vibrational mode, has so far prohibited the study of vibrational energy relaxation and/or spectral diffusion in AIMD simulations with periodic boundary conditions. As a result, the application of AIMD simulations has been limited to computing the static vibrational spectra of water and solutes in water [31–35]. On the other hand, some pioneering classical force-field nonequilibrium MD (NEMD) simulations have succeeded in computing the vibrational dynamics followed by the vibrational excitation by tracing the excess kinetic energy relaxation [36–46] as well as the electrostatic mapping technique [47]; however, they may present a biased view as they do not account for the anharmonicity and delocalization of the vibrational modes from electronic structure theory, which is, in particular, critical for the O-H stretch mode in bulk H_2O.

In classical MD simulations, the optical excitation can be readily simulated by applying an external electric field $\boldsymbol{E}$ oscillating with frequency ω to a system [39]. For an empirical force-field model with point charges, the force acting on the atoms, $\boldsymbol{F}$, can be evaluated by $\boldsymbol{F} = -q\boldsymbol{E}$, where q is the charge of the corresponding atom. Since a continuous charge density is used instead of point charges in AIMD simulations, adding the external electric-field term to the AIMD Hamiltonian raises a conflict with the periodic boundary conditions. To resolve this, a complex treatment of an external electric field with the Berry phase approach is required [48,49]. Such complications in AIMD simulations can be circumvented using a reverse NEMD (RNEMD) technique, where the atom velocities are swapped in the absence of an external field [50,51]. Since a nonequilibrium state generated by using the original RNEMD technique does not contain frequency-resolved information, the RNEMD algorithm should be extended so that the velocity-swapping operation is controlled with specific frequency.

In this study, we develop a RNEMD algorithm to generate a frequency-resolved nonequilibrium state and elucidate the mechanism of the spectral diffusion of the O-H stretch mode in liquid H_2O. By using this RNEMD algorithm, we excite the O-H stretch mode with AIMD simulations. Then, we compute the excess velocity correlation function (VCF) from the difference between the RNEMD and equilibrium MD (EMD) trajectories and track the time variations of the excess VCF intensity in the frequency domain [39]. Eliminating velocity cross correlations between different O-H chromophores in the VCF spectra allows us to explore the effect of the delocalization of the O-H stretch mode over several O-H chromophores on the spectral diffusion dynamics. Furthermore, by tracking energy transfer from excited O-H groups or excited H_2O molecules to specific non-excited O-H chromophore subgroups, we elucidate the contributions of the intramolecular and intermolecular energy transfer of the localized O-H stretch.

II. RESULTS

A. Center of mass frequency dynamics of O-H stretch in H_2O

The delocalization of the O-H stretch chromophore significantly affects the infrared (IR) spectrum of bulk H_2O. The IR spectra of H_2O are represented by the Fourier transform of the velocity correlation function (VCF) via Eqs. (13) and (15) (in Sec. IV B) [52], and the delocalization of the O-H chromophores is contained in the cross terms of the VCF, as demonstrated in Sec. IV. To examine the effect of the delocalized O-H stretch mode on the static VCF spectrum in our AIMD simulation, we calculated the Fourier-transformed VCF from the equilibrium MD (EMD) trajectory, $R^{EMD}(\omega; r_t)$, with various cross-correlation truncation radii, r_t, in Eq. (13). These are shown in Fig. 1. The
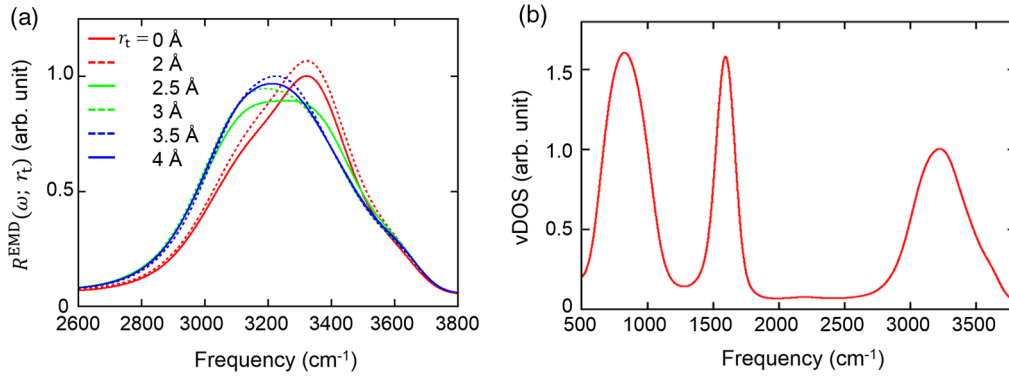
FIG. 1.   (a) Calculated Fourier-transformed VCF spectra in the O-H stretch region. Variations of the Fourier-transformed VCF spectra $R^{\text{EMD}}(\omega; r_t)$ with various truncation radii r_t. Note the increasing redshift with increasing r_t (i.e., delocalization), almost saturating at $r_t = 3.5$ Å. (b) Calculated Fourier-transformed VCF spectra in the spectral region ($500 - 3800$ cm^{-1}) with $r_t = 4.0$ Å.

peak of the VCF spectrum appears to be redshifted with increasing r_t, indicating that, as expected, delocalization of the O-H stretch chromophores amplifies the vibrational density of states at about 3200 cm^{-1} by coupling to the lower-frequency O-H stretching modes intermolecularly. This result is consistent with IR spectra calculated from classical MD simulations [53] and electrostatic mapping [7]. However, the spatial extent of the delocalization is fairly limited: Figure 1 shows that the simulated VCF is almost independent of r_t at $r_t > 3.5$ Å, indicating that delocalization is restricted to the first hydration shell of the O-H chromophore, which is consistent with the simulations of larger liquid water systems [34,53]. Additionally, we plotted the VCF with the cutoff of $r_t = 4$ Å in the frequency range of 500 cm^{-1} < ω < 3800 cm^{-1}, indicating that our simulation also reproduces the bending and librational modes, in addition to the OH stretching mode.

Then, we added the excess kinetic energy to the 3600 cm^{-1} O-H stretch mode by swapping the velocities of the O and H atoms every 4.63 fs with the RNEMD algorithm developed in this study. The details of the algorithm can be found in the Sec. IV.The time interval of 4.63 fs for the momentum-swapping operation defines the excitation frequency of 3600 cm^{-1} via Eq. (8) (in Sec. IV B). We monitor the subsequent spectral diffusion by computing the time variations of the center of mass (COM) frequency for the excess VCF spectra with $r_t = 4$ Å via Eq. (16). The decays of the COM frequency, which are a direct measure of spectral diffusion of the O-H stretch mode in bulk H$_2$O, are shown in Fig. 2. A mono-exponential fit to the COM decay yields a decay time of 140 ± 44 fs for $r_t = 4$ Å, which is in good agreement with the recent experiments, reporting 176 ± 39 fs [16] and simulations (140 fs) [40]. Thus, the simulated COM frequency at the the Becke exchange functional [54] and Lee-Yang-Parr correlation functional [55] (BLYP)/the double-zeta valence polarized basis set (DZVP) level of the theory with the dispersion correction [56] reproduces the

experimental data very well. Note that the temperature increase due to the RNEMD is less than 1.3 K, which is smaller than the experimental value of 3 K [16], indicating that the temperature increase in our simulation can be considered as a small perturbation.

B. Localized vs delocalized vibrational mode for spectral diffusion

The results presented in Fig. 1 illustrate that the O-H stretch vibration is significantly delocalized, causing a redshift in the spectrum. This delocalization of the O-H stretch chromophore accelerates the spectral diffusion in bulk H$_2$O because frequency modulations of the
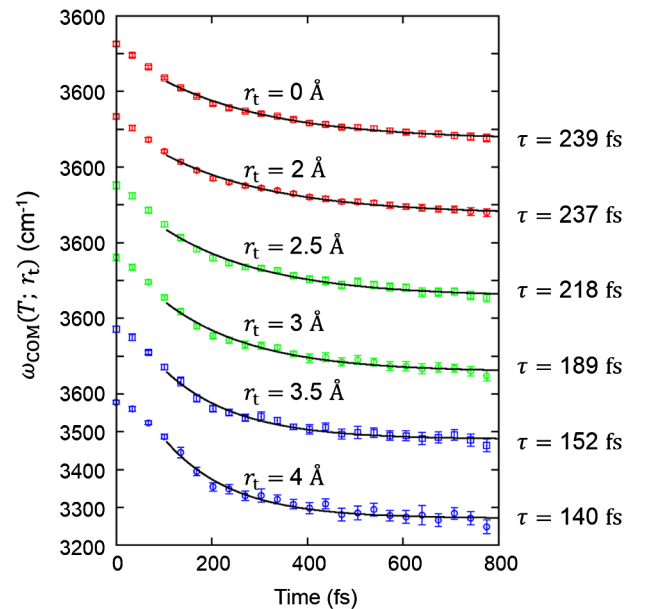

FIG. 2.   Spectral diffusion of the O-H stretch vibration, which slows down as delocalization is decreased. We show time traces of the COM frequency $\omega_{\text{COM}}(T; r_t)$ with various truncation radii r_t. Mono-exponential fits (solid black lines) demonstrate about a twofold slow-down of the spectral diffusion as the delocalization of vibrational energy is progressively switched off ($r_t \rightarrow 0$ Å).

delocalized O-H chromophore occur not only from hydrogen-bond fluctuations of a single O-H group but also from the fluctuations of the hydrogen bonds in the first hydration shell. Note that such fluctuations also include modulation of the vibrational frequency due to nonresonant coupling to lower-frequency modes (e.g., librations). Here, we examine the effect of the delocalization of the vibrational mode on the spectral diffusion. To this end, we decouple the vibrational modes of the neighboring O-H chromophores by decreasing the truncation radius r_t, and we simulate the COM frequency dynamics. Note that in this manner, we "switch off" delocalization but not intramolecular or intermolecular energy transfer between individual localized O-H chromophores. As can be seen in Fig. 2, the dynamics of the COM frequencies slows down with decreasing r_t, indicating that, as expected, the delocalization of the O-H stretch mode contributes to the acceleration of the spectral diffusion of H_2O. The fit to the data gives the time constants of 152, 189, 218, 237, and 239 fs for $r_t = 3.5$, 3, 2.5, 2, and 0 Å, respectively. Since, for a given O-H chromophore, only the neighboring O-H group within the same H_2O molecule is included in the VCF calculation for $r_t = 2$ Å, the observation that similar time constants are obtained for $r_t = 2$ and 0 Å demonstrates that the two O-H stretch chromophores contained within the same water molecule are dynamically decoupled, and thus, intramolecular delocalization constitutes a negligible contribution to the spectral diffusion. In contrast to the limited impact of the coupling to the O-H chromophores contained within the same molecule on the spectral diffusion of H_2O, the delocalized O-H stretch chromophores generated via near-resonant intermolecular coupling has a higher impact. From the decrease in the time constants of the COM frequency decay by increasing r_t from 2 to 4 Å, it is evident that the delocalization of the vibrational mode accelerates the spectral diffusion by 41%. This is a direct consequence of hydrogen-bond fluctuations of several nearby O-H groups contributing to the spectral diffusion through the delocalization of the chromophores, in line with what has been suggested based on experiments [14,15].

However, the COM frequency for the localized O-H stretch mode ($r_t = 0$ Å) exhibits faster dynamics (0.24 ps) than the spectral diffusion of the (isolated) O-H stretch of HDO diluted in D_2O (0.5–1 ps) [19–23], indicating that the observed spectral diffusion for the localized mode is still much faster than the correlation decay due to fluctuation of the O-H stretch frequency alone; intramolecular or intermolecular energy-transfer events further accelerate the spectral diffusion in pure H_2O, in addition to the delocalization of the O-H stretch chromophore. Unlike the O-H chromophores of dilute HDO in D_2O, the vibrational energy of the O-H stretch chromophores may be transferred to the other O-H stretch chromophores in the H_2O, giving rise to changes in the vibrational frequency, thereby contributing to the spectral diffusion. This result is distinctly different from the delocalization described in the previous paragraph, in that intermolecular energy transfer will lead to a spatial migration of the (delocalized) vibrational exciton. In the next section, we investigate the effect of this intramolecular and intermolecular energy transfer on the spectral diffusion.

C. Effects of intramolecular and intermolecular energy transfer on spectral diffusion

The COM frequency decay for the excess VCF with $r_t = 0$ Å contains three possible contributions: the frequency correlation decay of the individual O-H stretch chromophore (single chromophore, sc), intramolecular energy transfer, and intermolecular energy transfer. When the time constants for these three mechanisms are denoted as τ_{sc}, τ_{intra}, and τ_{inter}, respectively, the time constant for the COM frequency decay for the localized O-H stretch chromophore of 239 ± 14 fs is related to these time constants as

$$\frac{1}{239 \text{ fs}} = \frac{1}{\tau_{sc}} + \frac{1}{\tau_{intra}} + \frac{1}{\tau_{inter}}. \qquad (1)$$

To study the intramolecular and intermolecular energy-transfer rates, we decomposed the 64 O-H stretch chromophores (32 water molecules in a simulation cell) into two distinct subgroups, one composed of higher-frequency O-H chromophores (G) and the other group containing the remaining O-H chromophores (G'), and we computed the time constant of the excess energy transfer with the frequency of 3600 cm^{-1} from subgroup G to G' in a cascading model via Eq. (18) (in Sec. IV C).

To disentangle intramolecular and intermolecular transfer, two different G subgroups (G1 and G2) are introduced. First, subgroup G1 is composed of the eight O-H chromophores with the highest vibrational frequencies, and subgroup G1' consists of the remaining 56 O-H chromophores. Since 3600 cm^{-1} is much higher than the peak frequency of 3274 cm^{-1} of the VCF spectrum, these eight O-H stretch chromophores with the highest O-H stretch frequency contain most of the O-H chromophores contributing to the VCF at about 3600 cm^{-1} [72% and 82% in the G1 and G2 subgroups, respectively, for the 3500–3700 cm^{-1} region at $T = 50$ fs; see Fig. 3(b)]. To select these top eight O-H stretch chromophores with high frequency, we computed the projected O-H stretch velocity $v^{pro,OH}(t) = \vec{v}^{OH}(t) \cdot \vec{r}^{OH}(t)$ and counted the number of sign changes of $v^{pro,OH}(t)$ during the first 880 MD steps. The eight O-H stretch chromophores that most frequently changed sign of $v^{pro,OH}(t)$ were assigned to the G1 group. If all eight O-H chromophores belong to different water molecules, the excess energy transfer from the G1 subgroup to the rest of the O-H stretch chromophores (G1') occurs both intermolecularly and intramolecularly; for any particular O-H groups, one chromophore is situated within the same water molecule and serves as a potential acceptor
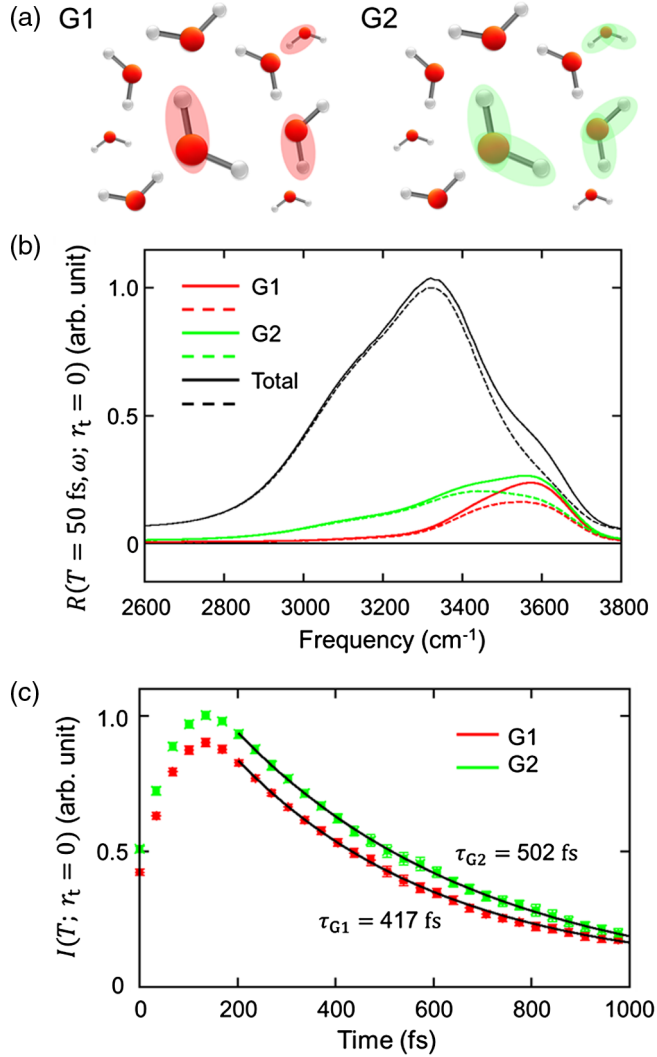
FIG. 3. Schemes to disentangle the effects of intramolecular and intermolecular energy transfer on spectral diffusion. (a) Schematic pictures of the G1 and G2 subgroups of the O-H chromophores. The rest of the O-H chromophores are assigned to the $G1'$ and $G2'$ subgroups, respectively. (b) Fourier-transformed VCF spectra for the RNEMD (solid line) and EMD (dashed line) at time $T = 50$ fs for the G1 and G2 subgroups. For comparison, the VCF spectra for all O-H chromophores are also plotted (Total). (c) Time dependence of the excess VCF intensities for the G1 and G2 subensembles.

in case of intramolecular energy transfer, while the remaining 62 chromophores are possible acceptors via intermolecular energy transfer. However, since 7 of the 62 potential acceptors are contained within subgroup G1, the time constant for the decay of the excess VCF intensity in G1 is given by

$$\frac{1}{\tau_{G1}} = \frac{1}{\tau_{intra}} + \frac{55}{62}\frac{1}{\tau_{inter}}. \qquad (2)$$

However, the O-H groups belonging to G1 are not necessarily all located in different water molecules. For

x O-H chromophores ($x = 0, 2, 4, 6,$ or 8) out of these eight G1 chromophores contained within the same water molecule, Eq. (2) can be generalized to

$$\frac{1}{\tau_{G1}} = \frac{8-x}{8}\frac{1}{\tau_{intra}} + \frac{55 + x/8}{62}\frac{1}{\tau_{inter}}. \qquad (3)$$

Next, we defined the G2 subgroup consisting of the eight O-H stretch chromophores assigned to the G1 subgroup plus the chromophores contained in the same water molecule as the G1 chromophores (i.e., G2 are the H_2O molecules that contain the eight O-H oscillators with the highest vibrational frequencies). In this categorization, the intramolecular energy transfer does not contribute to the energy transfer from the G2 subgroup to the $G2'$, unlike the energy transfer from the G1 to the $G1'$. The time constant of the excess energy transfer from the G2 subgroup to the rest of the O-H stretch chromophores ($G2'$) is given by

$$\frac{1}{\tau_{G2}} = \frac{48 + x}{62}\frac{1}{\tau_{inter}}, \qquad (4)$$

since only $48 + x$ out of the potential 62 acceptors are contained within $G2'$. By combining Eqs. (1), (3), and (4), the three time constants, τ_{sc}, τ_{intra}, and τ_{inter}, can be obtained, with τ_{G1} and τ_{G2} coming from the simulations. The schematic pictures of the G1 and G2 subgroups are depicted in Fig. 3(a). Note that since we select the topmost high-frequency O-H chromophores in the G subgroups, more O-H chromophores in the G subgroups contain lower-frequency O-H stretch chromophores. Since the lower-frequency O-H stretch modes spectrally overlap with the overtone of the H-O-H bend mode, vibrational energy in these modes can efficiently relax to the H-O-H bend mode, in addition to the energy relaxation pathway from the G to G' subgroups [9,16]. This energy relaxation pathway violates the cascading model assumption mentioned above. To avoid the contribution of this energy relaxation mechanism, we chose the eight high-frequency O-H chromophores.

The Fourier transformed VCF spectra for the RNEMD and EMD at time $T = 0$ fs are displayed in Fig. 3(b). These spectra show that the excess 3600 cm^{-1} VCF is indeed mostly covered by the G1 or G2 subgroup. Figure 3(c) shows the time traces for the excess VCF intensities $I(T; r_t = 0$ Å$)$ for G1 and G2. The mono-exponential fits give the time constants of $\tau_{G1} = 417 \pm 30$ fs and $\tau_{G2} = 502 \pm 35$ fs. The quantity x appearing in Eqs. (3) and (4) was calculated by counting the number of water molecules with two O-H stretch chromophores assigned to the G1 in the AIMD trajectory, and $x = 1.564$ is obtained. By inserting this x into Eqs. (1), (3), and (4), we obtained $\tau_{sc} = 680 \pm 170$ fs, $\tau_{intra} > 3.0$ ps, and $\tau_{inter} = 400 \pm 10$ fs.

As mentioned above, the structural relaxation τ_{sc} can be experimentally accessed by measuring the spectral

diffusion of isotopically diluted O-H stretch chromophores in D_2O, where intramolecular and intermolecular couplings are switched off and delocalization is negligible [23,57]. Our simulated $\tau_{sc} = 680 \pm 170$ fs is in good agreement with the experimental reports of 0.5–1 ps [19–23]. Our analysis indicates that intramolecular energy transfer contributes negligibly to the overall spectral diffusion. This implies that the frequencies of the two O-H stretching chromophores in a water molecule do not overlap significantly, which is in good agreement with the instantaneous asymmetric hydrogen bond structure in liquid water recently proposed by Kuhne and Zhaliullin [29]. It is thus evident that intermolecular coupling between O-H groups, both through delocalization of the vibrational amplitude and intermolecular energy transfer between the O-H groups, dominates spectral diffusion for the O-H stretch mode in H_2O.

Note that we do not take nuclear quantum effects [36–38,40,44–46] into account, i.e., the effect of the zero-point energy on vibrational dynamics. For the vibrational energy transfer, we consider only the energy transfer between the O-H stretch chromophores, while the variation of the zero-point energy for the O-H stretch mode is comparable to the thermal energy ($k_B T$), suggesting that the classical approximation holds [40,58–61]. Indeed, our results are in excellent agreement with the experimentally determined total spectral diffusion rate of neat H_2O, and our deduced time constant for structural relaxation is also in accordance with experiments on HOD in D_2O, indicating that nuclear quantum effects are not critical for the spectral diffusion process. To verify that nuclear quantum effects have little effect on our conclusions, we calculated the spectral diffusion rate by multiplying the VCF by the harmonic quantum corrections:

$$Q(\omega) = \beta\hbar\omega/[1 - \exp(-\beta\hbar\omega)]. \quad (5)$$

The calculated time constant for spectral diffusion amounts to 147 fs, which is very close to the value of 140 fs obtained without the quantum correction. This indicates that the quantum correction indeed plays a minor role for the spectral diffusion of the water's O-H stretch mode.

III. CONCLUSIONS

We have presented a new algorithm to generate a frequency-resolved nonequilibrium state by modifying the RNEMD technique, where the partial velocities of O and H atoms are swapped with a time interval corresponding to the excitation frequency. This technique is ideal for simulating the excitation of specific vibrational frequency in AIMD simulations with periodic boundary conditions. To clarify the molecular-level details of the spectral diffusion mechanism in bulk H_2O, we ran AIMD simulations at the BLYP/DZVP with the dispersion correction and excited at a frequency of 3600 cm^{-1}. The time constant

of the spectral diffusion inferred from the simulations of 140 fs is in good agreement with experimentally reported values. We subsequently examined the effects of the delocalization of the O-H stretch chromophores on the spectral diffusion of H_2O by varying the truncation radius of the cross-correlation function. Our results indicate that the coherently delocalized O-H stretch chromophore accelerates the spectral diffusion by 41%. We then surveyed the intramolecular and intermolecular energy transfer within the O-H stretch chromophores. Remarkably, though the two O-H oscillators within a water molecule are intrinsically strongly coupled, the analysis of our simulations shows that intramolecular energy transfer has a negligible contribution to the spectral diffusion. Intermolecular energy transfer, on the other hand, occurs on a 400-fs time scale. The calculated time constant for the frequency correlation decay of a single O-H stretch chromophore is 680 fs, again in good agreement with experimental data measured on the O-H stretch mode of HOD in D_2O. Our AIMD simulation with the modified RNEMD technique clearly shows that the delocalization and the intermolecular energy transfer of the O-H stretch chromophores can virtually explain the entire spectral dynamics and contribute nearly equally to the spectral diffusion of the O-H stretch mode in H_2O.

IV. METHODS

A. Reverse nonequilibrium MD algorithm for generating frequency-resolved excited states

To excite O-H stretch vibrations with a particular vibrational frequency, a nonequilibrium state with a specific frequency distribution needs to be generated within the AIMD simulation. Such a nonequilibrium state is generated by swapping the atom velocities without applying external forces. This technique is called the RNEMD approach [50,51]. However, with the original RNEMD algorithm, a generated nonequilibrium state is not frequency resolved. In this section, we extend this RNEMD algorithm to generate a frequency-resolved nonequilibrium state.

In the original RNEMD algorithm, the velocities are swapped every time interval t_s between atoms A and A$'$ as

$$v_{j,A}^{(+)} \rightarrow v_{j,A'}^{(-)}, \qquad v_{j,A'}^{(-)} \rightarrow v_{j,A}^{(+)}, \quad (6)$$

where $v_{j,i}^{(+)}(v_{j,i}^{(-)})$ are the positive (negative) velocities of atom i along direction j ($j = x, y, z$). By selecting the same atom species for atoms A and A$'$, the total momentum and energy are conserved before and after velocity swapping. This velocity-swapping procedure makes a nonequilibrium steady state but not a frequency-resolved nonequilibrium state.

To make a nonequilibrium state frequency resolved, the swapped momentum in a system was designed to obey a Gaussian envelope:

$$\sum_{A,A'} m_A \Delta v_{j,AA'} = M_0 \exp\left(-\frac{T^2}{2\sigma^2}\right) \cos(2\pi\omega_s T), \quad (7)$$

where M_0 is the maximum swapped momentum, $2\sqrt{2\ln 2}\,\sigma$ is the full width at half maximum of the Gaussian envelope, and $\Delta v_{j,AA'}$ is the j element of the swapped velocity between atoms A and A'. Note that $T = 0$ is set at the center of the Gaussian envelope. To specifically excite vibrational modes with frequency ω_s, the time interval t_s for the swapping velocity is

$$t_s = 1/2c\omega_s. \quad (8)$$

Equations (7) and (8) indicate that the sign of the total swapped momentum varies every t_s.

The swapped velocity is given by $\Delta v_{j,AA'} = v_{j,A}^{(+)} - v_{j,A'}^{(-)}$ when procedure expressed by Eq. (6) is employed, indicating that the amplitude of swapped velocities cannot be controlled. Hence, procedure (6) makes it difficult to satisfy Eq. (7). To control the swapped velocities exactly, partial velocities, $\Delta v_{j,A}$ and $\Delta v_{j,B}$, are swapped between four atoms A, A', B, and B' as

$$v_{j,A}^{(+)} \rightarrow (v_{j,A}^{(+)} + \Delta v_{j,AB'}),$$
$$v_{j,B'}^{(-)} \rightarrow (v_{j,B'}^{(-)} - m_A/m_{B'} \cdot \Delta v_{j,AB'}), \quad (9)$$

$$v_{j,B}^{(-)} \rightarrow (v_{j,B}^{(-)} + \Delta v_{j,BA'}),$$
$$v_{j,A'}^{(+)} \rightarrow (v_{j,A'}^{(+)} - m_B/m_{A'} \cdot \Delta v_{j,BA'}), \quad (10)$$

where m_i is the mass of the atom i, and the signs of $\Delta v_{j,AB'}$ and $\Delta v_{j,BA'}$ are set to be the same. $\Delta v_{j,AB'}$ and $\Delta v_{j,BA'}$ are computed to keep the total energy unchanged before and after velocity swapping to suppress any temperature change of the system. Note that the total momentum is also unchanged as is evident from the swapping procedures of (9) and (10). For bulk water, atoms A and B are set to be the hydrogen atoms, while atoms A' and B' are set to be the oxygen atoms. A schematic picture of the velocity swapping is depicted in Fig. 4(a).

For monitoring the vibrational dynamics, excess energy has conventionally been added to specific localized vibrational modes, and the time evolution of this excess energy has been monitored [37,38,44]. The advantages of our RNEMD technique over this technique are as follows. (1) The RNEMD technique can specify the excitation frequency, enabling us to monitor the spectral diffusion. (2) The RNEMD technique can excite both localized and delocalized modes, whereas this conventional technique can excite only well-defined localized vibrational modes such as the amide I mode in water [46,62] and O-H stretch in D_2O [59]. Since the delocalized O-H stretch mode critically affects the vibrational dynamics as mentioned in the Introduction, this technique is less appropriate for investigating the vibrational dynamics of the O-H stretch
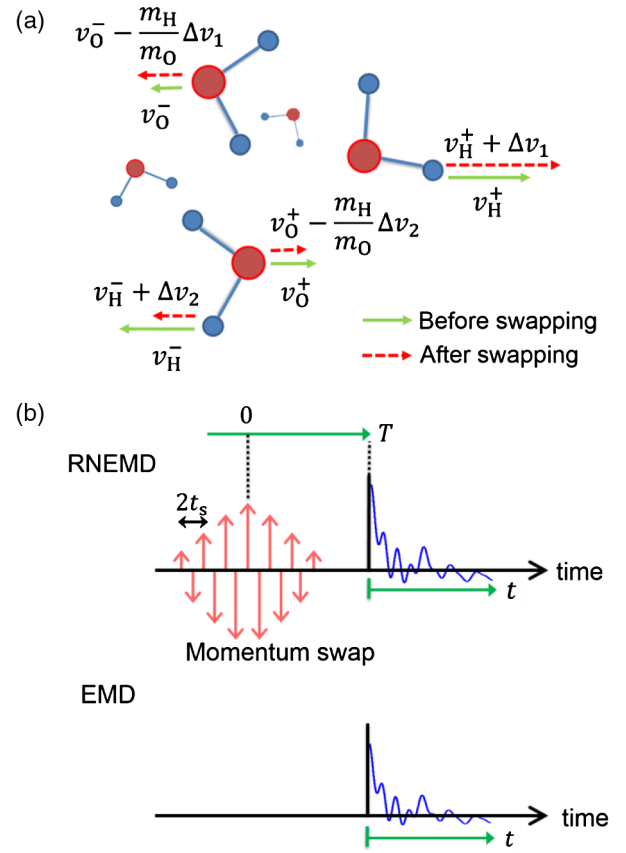

FIG. 4. Representation of the computational method. Schematic pictures of (a) swapping partial atom velocities in H_2O and (b) simulation procedures to calculate the VCFs from the RNEMD and EMD trajectories.

chromophore in H_2O. On the other hand, the conventional excess energy insertion technique can mimic the momentum distribution of the first excited state; the effects of the initial vibrational excitation on the vibrational dynamics have been examined in a model calculation and/or classical force-field MD simulation [38,44], while the initial state is generated by thermally exciting a vibrational mode in our RNEMD technique. The effects of thermal and quantum excitations on the vibrational dynamics have been examined in water by Rey and co-workers, showing insensitivity of the initial vibrational excitation to the vibrational dynamics [36,38]. Based on this result, we assume that the thermal excitation is independent of the initial vibrational excitation. Modeling the initial vibrational excitation would be the next challenge for the RNEMD algorithm developed here.

B. Velocity correlation function

After generating the frequency-resolved nonequilibrium state, the subsequent vibrational dynamics is monitored by computing the difference between Fourier-transformed VCFs for the (nonequilibrium, "excited") RNEMD and

(equilibrium, "ground-state") EMD trajectories [39]. The VCF for the O-H stretch mode is given by

$$R^{\text{RNEMD/EMD}}(T, t) = \left\langle \sum_{i,j} \sum_{k=x,y,z} v_{ki}^{\text{OH}}(t + T) v_{kj}^{\text{OH}}(T) \right\rangle,$$

(11)

where $v_{ki}^{\text{OH}}(t)$ represents the kth element of the relative velocity of the oxygen $[v_{ki}^{\text{O}}(t)]$ and hydrogen atoms $[v_{ki}^{\text{H}}(t)]$ for O-H chromophore i, $v_{ki}^{\text{OH}}(t) = v_{ki}^{\text{H}}(t) - v_{ki}^{\text{O}}(t)$ [52]. To enhance the efficiency of sampling, the Fourier-transformed VCFs are averaged over $-\Delta T < t < \Delta T$ as

$$R^{\text{RNEMD/EMD}}(T; t) = \left\langle \frac{1}{2\Delta T} \int_{-\Delta T}^{\Delta T} \sum_{i,j} \sum_{k=x,y,z} v_{ki}^{\text{OH}}(t + T + t') v_{kj}^{\text{OH}}(T + t') dt' \right\rangle,$$

(12)

where ΔT was set to 16.8 fs (40 MD steps).

To examine the contribution of the delocalization of the excitation over different O-H chromophores [6,7], we introduced the spatially truncated formalism of the VCF [53,62]:

$$R^{\text{RNEMD/EMD}}(T, t; r_{\text{t}}) = \left\langle \frac{1}{2\Delta T} \int_{-\Delta T}^{\Delta T} \sum_{i,j} \sum_{k=x,y,z} v_{ki}^{\text{OH}}(t + T + t') v_{kj}^{\text{OH}}(T + t') g_{\text{t}}(r_{ij}(T + t'); r_{\text{t}}) dt' \right\rangle,$$

(13)

where $r_{ij}(t)$ is the distance between O-H chromophores i and j at time t, and a truncating function $g_{\text{t}}(r, r_{\text{t}})$ is given by

$$g_{\text{t}}(r; r_{\text{t}}) = \begin{cases} 1 & \text{for } r \leq r_{\text{t}} \\ 0 & \text{for } r > r_{\text{t}} \end{cases}.$$

(14)

$R^{\text{RNEMD/EMD}}(T, t; r_{\text{t}} = 0)$ is the velocity autocorrelation function of the O-H stretch chromophores arising from the localized O-H chromophores, while the cross correlations $\langle \sum_{i \neq j} v_i^{\text{OH}}(t + T) v_j^{\text{OH}}(T) \rangle$ account for delocalization of the O-H stretch chromophores. The excess energy in the localized O-H chromophores corresponds to the added kinetic energy. Thus, it provides information on (incoherent) energy transfer between oscillators, while the cross-correlation terms represent the coherence of the O-H vibrations. Note that the VCF for the EMD trajectory, $R^{\text{EMD}}(T, t; r_{\text{t}})$, for the whole O-H stretch chromophores is independent of T, whereas the EMD VCF spectra for the G subgroup change in time, which has to be taken into account for the excess VCF in the RNEMD/EMD calculations (see below).

The Fourier-transformed VCF for the RNEMD trajectory at time T can be calculated as

$$R^{\text{RNEMD/EMD}}(T; \omega)$$
$$= \int_0^\infty \cos(\omega t) R^{\text{RNEMD/EMD}}(T; t) f(t) dt,$$

(15)

where $f(t)$ is the Hann window function:

$$f(t) = \begin{cases} \cos^2(\pi t/2t_0) & \text{for } 0 < t < t_0 \\ 0 & \text{for } t > t_0 \end{cases},$$

(16)

The end time of the Hann window function, t_0, was set to 281.8 fs (669 MD steps). The simulation procedures of $R^{\text{RNEMD/EMD}}(T; t)$ are given in the next section. Schematic representations of these simulation protocols are shown in Fig. 4(b).

C. Computation of center-of-mass frequency dynamics and energy-transfer dynamics

Information on the spectral diffusion has been extracted experimentally from the decay of the center line slope (CLS) [16,63] and the nodal line slope (NLS) [13,41] separating the peaks arising from the $1 \rightarrow 2$ and $1 \rightarrow 0$ transitions in the 2D spectroscopy. In the limit where the spectral diffusion is statistical, that is, with a directionality given by the spectral intensity distribution, equivalent information on the CLS and NLS can be obtained from the COM frequency [64]. Since no strong frequency dependence of the spectral diffusion has been experimentally observed for the O-H stretch mode in bulk water [16], we computed the time constant of the spectral diffusion from the time trace of the COM frequency by exciting a 3600 cm^{-1} O-H stretch mode. The time variation of the COM frequency can be calculated from the VCF as

$$\omega_{\text{COM}}(T; r_{\text{t}})$$
$$= \frac{\int_{\omega_1}^{\omega_2} \omega'(R^{\text{RNEMD}}(T, \omega'; r_{\text{t}}) - R^{\text{EMD}}(\omega'; r_{\text{t}})) d\omega'}{\int_{\omega_1}^{\omega_2} (R^{\text{RNEMD}}(T, \omega'; r_{\text{t}}) - R^{\text{EMD}}(\omega'; r_{\text{t}})) d\omega'},$$

(17)

where ω_1 (ω_2) denotes the lower (upper) limit of the frequency for the vibrational mode under consideration. For the O-H stretch mode of H_2O, we set $\omega_1 = 2800$ cm^{-1} and to cover the whole O-H stretch mode peak in the VCF spectrum. Note that since the shape of the spectrum affects both the numerator and denominator of Eq. (17) in the same manner, the COM dynamics is insensitive to the spectral line shape. Accordingly, as shown in Fig. 2, the COM frequencies after long T are indistinguishable within the error bars for different r_t.

The energy transfer from the G subgroup to the other subgroup G′ (see Results) can be monitored in time by calculating the time variation of the excess spectral intensity of the excess VCF for the G subgroup (G = G1, G2) as [39]

$$I(T; r_t) = \int_{\omega_1}^{\omega_2} (R_G^{\text{RNEMD}}(T, \omega'; r_t) - R_G^{\text{EMD}}(T, \omega'; r_t))d\omega',$$

$$(18)$$

where $R_G^{\text{RNEMD/EMD}}(T, \omega'; r_t)$ is the Fourier-transformed VCF for the G subgroup calculated from the RNEMD/EMD trajectories.

D. *Ab initio* molecular dynamics

We used the CP2K code [65,66] for the AIMD runs. The BLYP functional [54,55] was used for the exchange and correlation functional, and core electrons were described by the norm-conserving Goedecker-Teter-Hutter (GTH) pseudopotential [67]. We used the DZVP basis set. A charge-density cutoff of 280 Ry was employed for the real-space grid with density smoothing. The simulation cell contained 32 H_2O molecules, and the density of water was set to 0.997 g/cm^3. We used the time step of 0.421 fs for integrating equations of motion.

Using a snapshot of the water molecules obtained from a classical MD simulation with the TIP3P model, we started a 3-ps AIMD simulation by rescaling the atom velocities. Then, we ran a 10-ps AIMD simulation in the NVT ensemble with the Nose-Hoover thermostat and the sequential 10-ps AIMD simulation in the NVE ensemble to equilibrate the system. Afterwards, a 190-ps AIMD simulation was conducted from which 15000 snapshots were obtained. These were used as the initial coordinates and velocities for the reverse nonequilibrium AIMD (RNEAIMD) runs. The average temperature in the 190-ps AIMD simulation was 316.8 K.

E. Reverse nonequilibrium molecular dynamics

We applied the RNEMD methodology developed here to the AIMD simulation to explore the mechanism of spectral diffusion for the O-H stretch mode in the neat bulk H_2O by enhancing the amplitudes of (exciting) the 3600 cm^{-1} vibrational mode. We conducted 15000 RNEAIMD runs

to obtain the perturbed AIMD trajectories. In the RNEAIMD run, the atom velocities were swapped every 11 MD steps for the first 880 MD steps, and subsequently, 2800 MD steps were obtained after the perturbation. The amplitude of the total momentum swap was set as $M_0 = 1.210 \times 10^{-4}$ a.u., while σ was set to 100 fs, corresponding to a 62-cm^{-1} bandwidth for the excitation. We randomly selected 25–100 pairs consisting of two oxygen and two hydrogen atoms and swapped the atom velocities among these four atoms to obey the Gaussian envelope of the swapped momentum given by Eq. (7).

[1] I. Ohmine and H. Tanaka, *Fluctuation, Relaxations, and Hydration in Liquid Water. Hydrogen-Bond Rearrangement Dynamics*, Chem. Rev. **93**, 2545 (1993).

[2] P. Ball, *Water as an Active Constituent in Cell Biology*, Chem. Rev. **108**, 74 (2008).

[3] R. N. Butler and A. G. Coyne, *Water: Nature's Reaction Enforcers Comparative Effects for Organic Synthesis "In-Water" and "On-Water,"* Chem. Rev. **110**, 6302 (2010).

[4] D. Thirumalai, G. Reddy, and J. E. Straub, *Role of Water in Protein Aggregation and Amyloid Polymorphism*, Acc. Chem. Res. **45**, 83 (2012).

[5] S. Woutersen and H. J. Bakker, *Resonant Intermolecular Transfer of Vibrational Energy in Liquid Water*, Nature (London) **402**, 507 (1999).

[6] V. Buch, T. Tarbuck, G. L. Richmond, I. Groenzin, I. Li, and M. J. Shultz, *Sum Frequency Generation Surface Spectra of Ice, Water, and Acid Solution Investigated by an Exciton Model*, J. Chem. Phys. **127**, 204710 (2007).

[7] B. M. Auer and J. L. Skinner, *IR and Raman Spectra of Liquid Water: Theory and Interpretation*, J. Chem. Phys. **128**, 224511 (2008).

[8] H. J. Bakker and J. L. Skinner, *Vibrational Spectroscopy as a Probe of Structure and Dynamics in Liquid Water*, Chem. Rev. **110**, 1498 (2010).

[9] A. J. Lock and H. J. Bakker, *Temperature Dependence of Vibrational Relaxation in Liquid H_2O*, J. Chem. Phys. **117**, 1708 (2002).

[10] S. Ashihara, N. Huse, A. Espagne, E. T. J. Nibbering, and T. Elsaesser, *Vibrational Couplings and Ultrafast Relaxation of the O–H Bending Mode in Liquid H_2O*, Chem. Phys. Lett. **424**, 66 (2006).

[11] J. Lindner, P. Vöhringer, M. S. Pshenichnikov, D. Cringus, D. A. Wiersma, and M. Mostovoy, *Vibrational Relaxation of Pure Liquid Water*, Chem. Phys. Lett. **421**, 329 (2006).

[12] C.-S. Hsieh, R. K. Campen, M. Okuno, E. H. G. Backus, Y. Nagata, and M. Bonn, *Mechanism of Vibrational Energy*

Dissipation of Free OH Groups at the Air–Water Interface, Proc. Natl. Acad. Sci. U.S.A. **110,** 18780 (2013).

[13] P. Hamm and M. T. Zanni, *Concepts and Methods of 2D Infrared Spectroscopy* (Cambridge University Press, Cambridge, England, 2011).

[14] M. L. Cowan, B. D. Bruner, N. Huse, J. R. Dwyer, B. Chugh, E. T. J. Nibbering, T. Elsaesser, and R. J. D. Miller, *Ultrafast Memory Loss and Energy Redistribution in the Hydrogen Bond Network of Liquid* H_2O, Nature (London) **434,** 199 (2005).

[15] D. Kraemer, M. L. Cowan, A. Paarmann, N. Huse, E. T. J. Nibbering, T. Elsaesser, and R. J. D. Miller, *Temperature Dependence of the Two-Dimensional Infrared Spectrum of Liquid* H_2O, Proc. Natl. Acad. Sci. U.S.A. **105,** 437 (2008).

[16] K. Ramasesha, L. De Marco, A. Mandal, and A. Tokmakoff, *Water Vibrations Have Strongly Mixed Intra- and Inter-molecular Character,* Nat. Chem. **5,** 935 (2013).

[17] C. Fecko, J. Eaves, J. Loparo, A. Tokmakoff, and P. Geissler, *Ultrafast Hydrogen-Bond Dynamics in the Infra-red Spectroscopy of Water,* Science **301,** 1698 (2003).

[18] J. B. Asbury, T. Steinel, C. Stromberg, S. A. Corcelli, C. P. Lawrence, J. L. Skinner, and M. D. Fayer, *Water Dynamics: Vibrational Echo Correlation Spectroscopy and Compari-son to Molecular Dynamics Simulations,* J. Phys. Chem. A **108,** 1107 (2004).

[19] C. J. Fecko, J. J. Loparo, S. T. Roberts, and A. Tokmakoff, *Local Hydrogen Bonding Dynamics and Collective Reor-ganization in Water: Ultrafast Infrared Spectroscopy of* HOD/D_2O, J. Chem. Phys. **122,** 054506 (2005).

[20] R. Laenen, C. Rauscher, and A. Laubereau, *Dynamics of Local Substructures in Water Observed by Ultrafast Infra-red Hole Burning,* Phys. Rev. Lett. **80,** 2622 (1998).

[21] G. Gale, G. Gallot, F. Hache, N. Lascoux, S. Bratos, and J.-C. Leicknam, *Femtosecond Dynamics of Hydrogen Bonds in Liquid Water: A Real Time Study,* Phys. Rev. Lett. **82,** 1068 (1999).

[22] S. Woutersen and H. J. Bakker, *Hydrogen Bond in Liquid Water as a Brownian Oscillator,* Phys. Rev. Lett. **83,** 2077 (1999).

[23] C. P. Lawrence and J. L. Skinner, *Vibrational Spectroscopy of HOD in Liquid* D_2O. *III. Spectral Diffusion, and Hydrogen-Bonding and Rotational Dynamics,* J. Chem. Phys. **118,** 264 (2003).

[24] T. l. C. Jansen, B. M. Auer, M. Yang, and J. L. Skinner, *Two-Dimensional Infrared Spectroscopy and Ultrafast Anisotropy Decay of Water,* J. Chem. Phys. **132,** 224503 (2010).

[25] C.-S. Hsieh, M. Okuno, J. Hunger, E. H. G. Backus, Y. Nagata, and M. Bonn, *Aqueous Heterogeneity at the Air/Water Interface Revealed by 2D-HD-SFG Spectroscopy,* Angew. Chem. Int. Ed. **53,** 8146 (2014).

[26] M. D. Fayer, *Ultrafast Infrared Vibrational Spectroscopy* (CRC Press, Boca Ratan, 2013).

[27] R. Car and M. Parrinello, *Unified Approach for Molecular Dynamics and Density-Functional Theory,* Phys. Rev. Lett. **55,** 2471 (1985).

[28] D. Marx and J. Hutter, *Ab Initio Molecular Dynamics: Basic Theory and Advanced Methods* (Cambridge University Press, Cambridge, England, 2009).

[29] T. D. Kühne and R. Z. Khaliullin, *Electronic Signature of the Instantaneous Asymmetry in the First Coordination Shell of Liquid Water,* Nat. Commun. **4,** 1450 (2013).

[30] C. Zhang, R. Z. Khaliullin, D. Bovi, and L. Guidoni, *Vibrational Signature of Water Molecules in Asymmetric Hydrogen Bonding Environments,* J. Phys. Chem. Lett. **4,** 3245 (2013).

[31] P. L. Silvestrelli, M. Bernasconi, and M. Parrinello, *Ab Initio Infrared Spectrum of Liquid Water,* Chem. Phys. Lett. **277,** 478 (1997).

[32] M.-P. Gaigeot and M. Sprik, *Ab Initio Molecular Dynamics Computation of the Infrared Spectrum of Aqueous Uracil,* J. Phys. Chem. B **107,** 10344 (2003).

[33] H.-S. Lee and M. E. Tuckerman, *Dynamical Properties of Liquid Water from Ab Initio Molecular Dynamics Performed in the Complete Basis Set Limit,* J. Chem. Phys. **126,** 164501 (2007).

[34] M. Heyden, J. Sun, S. Funkner, G. Mathias, H. Forbert, M. Havenith, and D. Marx, *Dissecting the THz Spectrum of Liquid Water from First Principles via Correlations in Time and Space,* Proc. Natl. Acad. Sci. U.S.A. **107,** 12068 (2010).

[35] M. Sulpizi, M. Salanne, M. Sprik, and M.-P. Gaigeot, *Vibrational Sum Frequency Generation Spectroscopy of the Water Liquid–Vapor Interface from Density Functional Theory-Based Molecular Dynamics Simulations,* J. Phys. Chem. Lett. **4,** 83 (2013).

[36] R. Rey and J. T. Hynes, *Tracking Energy Transfer from Excited to Accepting Modes: Application to Water Bend Vibrational Relaxation,* Phys. Chem. Chem. Phys. **14,** 6332 (2012).

[37] F. Ingrosso, R. Rey, T. Elsaesser, and J. T. Hynes, *Ultrafast Energy Transfer from the Intramolecular Bending Vibration to Librations in Liquid Water,* J. Phys. Chem. A **113,** 6657 (2009).

[38] R. Rey, F. Ingrosso, T. Elsaesser, and J. T. Hynes, *Pathways for* H_2O *Bend Vibrational Relaxation in Liquid Water,* J. Phys. Chem. A **113,** 8949 (2009).

[39] T. Yagasaki and S. Saito, *A Novel Method for Analyzing Energy Relaxation in Condensed Phases using Nonequili-brium Molecular Dynamics Simulations: Application to the Energy Relaxation of Intermolecular Motions in Liquid Water,* J. Chem. Phys. **134,** 184503 (2011).

[40] S. Imoto, S. S. Xantheas, and S. Saito, *Ultrafast Dynamics of Liquid Water: Frequency Fluctuations of the OH Stretch and the HOH Bend,* J. Chem. Phys. **139,** 044503 (2013).

[41] T. Yagasaki and S. Saito, *Ultrafast Intermolecular Dynamics of Liquid Water: A Theoretical Study on Two-Dimensional Infrared Spectroscopy,* J. Chem. Phys. **128,** 154521 (2008).

[42] T. Hasegawa and Y. Tanimura, *Nonequilibrium Molecular Dynamics Simulations with a Backward-Forward Trajec-tories Sampling for Multidimensional Infrared Spectros-copy of Molecular Vibrational Modes,* J. Chem. Phys. **128,** 064511 (2008).

[43] Y. Nagata and Y. Tanimura, *Two-Dimensional Raman Spectra of Atomic Solids and Liquids,* J. Chem. Phys. **124,** 024508 (2006).

[44] P. H. Nguyen and G. Stock, *Nonequilibrium Molecular-Dynamics Study of the Vibrational Energy Relaxation of Peptides in Water,* J. Chem. Phys. **119,** 11350 (2003).

[45] G. Stock, *Classical Simulation of Quantum Energy Flow in Biomolecules*, Phys. Rev. Lett. **102**, 118301 (2009).

[46] H. Fujisaki and G. Stock, *Dynamic Treatment of Vibrational Energy Relaxation in a Heterogeneous and Fluctuating Environment*, J. Chem. Phys. **129**, 134110 (2008).

[47] A. Paarmann, T. Hayashi, S. Mukamel, and R. J. D. Miller, *Probing Intermolecular Couplings in Liquid Water with Two-Dimensional Infrared Photon Echo Spectroscopy*, J. Chem. Phys. **128**, 191103 (2008).

[48] R. King-Smith and D. Vanderbilt, *Theory of Polarization of Crystalline Solids*, Phys. Rev. B **47**, 1651 (1993).

[49] P. Umari and A. Pasquarello, *Ab Initio Molecular Dynamics in a Finite Homogeneous Electric Field*, Phys. Rev. Lett. **89**, 157602 (2002).

[50] F. Müller-Plathe, *A Simple Nonequilibrium Molecular Dynamics Method for Calculating the Thermal Conductivity*, J. Chem. Phys. **106**, 6082 (1997).

[51] F. Müller-Plathe, *Reversing the Perturbation in Nonequilibrium Molecular Dynamics: An Easy Way to Calculate the Shear Viscosity of Fluids*, Phys. Rev. E **59**, 4894 (1999).

[52] J. Liu, W. H. Miller, F. Paesani, W. Zhang, and D. A. Case, *Quantum Dynamical Effects in Liquid Water: A Semiclassical Study on the Diffusion and the Infrared Absorption Spectrum*, J. Chem. Phys. **131**, 164509 (2009).

[53] Y. Nagata and S. Mukamel, *Vibrational Sum-Frequency Generation Spectroscopy at the Water/Lipid Interface: Molecular Dynamics Simulation Study*, J. Am. Chem. Soc. **132**, 6434 (2010).

[54] A. D. Becke, *Density-Functional Exchange-Energy Approximation with Correct Asymptotic Behavior*, Phys. Rev. A **38**, 3098 (1988).

[55] C. Lee, W. Yang, and R. G. Parr, *Development of the Colle-Salvetti Correlation-Energy Formula into a Functional of the Electron Density*, Phys. Rev. B **37**, 785 (1988).

[56] S. Grimme, *Semiempirical GGA-Type Density Functional Constructed with a Long-Range Dispersion Correction*, J. Comput. Chem. **27**, 1787 (2006).

[57] B. M. Auer, R. Kumar, J. R. Schmidt, and J. L. Skinner, *Hydrogen Bonding and Raman, IR, and 2D-IR Spectroscopy of Dilute HOD in Liquid* D_2O, Proc. Natl. Acad. Sci. U.S.A. **104**, 14215 (2007).

[58] R. Rey, K. B. Møller, and J. T. Hynes, *Hydrogen Bond Dynamics in Water and Ultrafast Infrared Spectroscopy*, J. Phys. Chem. A **106**, 11993 (2002).

[59] K. B. Møller, R. Rey, and J. T. Hynes, *Hydrogen Bond Dynamics in Water and Ultrafast Infrared Spectroscopy: A Theoretical Study*, J. Phys. Chem. A **108**, 1275 (2004).

[60] B. S. Mallik, A. Semparithi, and A. Chandra, *Vibrational Spectral Diffusion and Hydrogen Bond Dynamics in Heavy Water from First Principles*, J. Phys. Chem. A **112**, 5104 (2008).

[61] B. S. Mallik, A. Semparithi, and A. Chandra, *A First Principles Theoretical Study of Vibrational Spectral Diffusion and Hydrogen Bond Dynamics in Aqueous Ionic Solutions:* D_2O *in Hydration Shells of* Cl^- *Ions*, J. Chem. Phys. **129**, 194512 (2008).

[62] Y. Nagata, C.-S. Hsieh, T. Hasegawa, J. Voll, E. H. G. Backus, and M. Bonn, *Water Bending Mode at the Water–Vapor Interface Probed by Sum-Frequency Generation Spectroscopy: A Combined Molecular Dynamics Simulation and Experimental Study*, J. Phys. Chem. Lett. **4**, 1872 (2013).

[63] K. Kwak, S. Park, I. J. Finkelstein, and M. D. Fayer, *Frequency-Frequency Correlation Functions and Apodization in Two-Dimensional Infrared Vibrational Echo Spectroscopy: A New Approach*, J. Chem. Phys. **127**, 124503 (2007).

[64] S. T. Roberts, K. Ramasesha, and A. Tokmakoff, *Structural Rearrangements in Water Viewed Through Two-Dimensional Infrared Spectroscopy*, Acc. Chem. Res. **42**, 1239 (2009).

[65] The CP2K developers group, http://www.cp2k.org/.

[66] J. VandeVondele, M. Krack, F. Mohamed, M. Parrinello, T. Chassaing, and J. Hutter, *Quickstep: Fast and Accurate Density Functional Calculations using a Mixed Gaussian and Plane Waves Approach*, Comput. Phys. Commun. **167**, 103 (2005).

[67] S. Goedecker, M. Teter, and J. Hutter, *Separable Dual-Space Gaussian Pseudopotentials*, Phys. Rev. B **54**, 1703 (1996).